Phys XXX: Superconductivity March 2013
University of Camerino

http://www.ualberta.ca/~fm3/courses/Camerino_Lectures/lecture_introduction.pdf

Superconductivity
and Strongly Correlated Electrons

F. Marsiglio
fm3@ualberta.ca

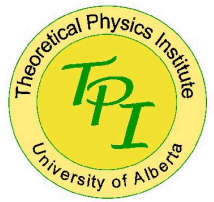

See arXiv:cond-mat/0106143

or Bennemann and Ketterson,
Superconductivity: Conventional and Unconventional Superconductors,
chapter 4, FM and J.P. Carbotte

$$\Sigma(\mathbf{k}, i\omega_m) \equiv \frac{1}{N\beta}\sum_{\mathbf{k}',m'} \frac{\lambda_{\mathbf{k}\mathbf{k}'}(i\omega_m - i\omega_{m'})}{N(\mu)} G(\mathbf{k}', i\omega_{m'}) \tag{42}$$

$$\phi(\mathbf{k}, i\omega_m) \equiv \frac{1}{N\beta}\sum_{\mathbf{k}',m'} \left[\frac{\lambda_{\mathbf{k}\mathbf{k}'}(i\omega_m - i\omega_{m'})}{N(\mu)} - V_{\mathbf{k}\mathbf{k}'}\right] F(\mathbf{k}', i\omega_{m'}), \tag{43}$$

$$G(\mathbf{k}, i\omega_m) = \frac{G_n^{-1}(\mathbf{k}, i\omega_m)}{G_n^{-1}(\mathbf{k}, i\omega_m)G_n^{-1}(-\mathbf{k}, -i\omega_m) + \phi(\mathbf{k}, i\omega_m)\bar{\phi}(\mathbf{k}, i\omega_m)} \tag{44}$$

$$F(\mathbf{k}, i\omega_m) = \frac{\phi(\mathbf{k}, i\omega_m)}{G_n^{-1}(\mathbf{k}, i\omega_m)G_n^{-1}(-\mathbf{k}, -i\omega_m) + \phi(-\mathbf{k}, -i\omega_m)\bar{\phi}(-\mathbf{k}, -i\omega_m)} \tag{45}$$

$$G_n^{-1}(\mathbf{k}, i\omega_m) = G_\circ^{-1}(\mathbf{k}, i\omega_m) - \Sigma(\mathbf{k}, i\omega_m). \tag{46}$$

where

$$\lambda_{\mathbf{k}\mathbf{k}'}(z) \equiv \int_0^\infty \frac{2\nu\alpha^2_{\mathbf{k}\mathbf{k}'}F(\nu)}{\nu^2 - z^2} d\nu$$

$$G_\circ(\mathbf{k}, i\omega_m) = [i\omega_m - (\epsilon_\mathbf{k} - \mu)]^{-1}$$

$$D_\circ(\mathbf{q}, i\nu_n) = [-M(\omega^2(\mathbf{q}) + \nu_n^2)]^{-1}$$

phonons

$$D(\mathbf{q}, i\nu_n) = \int_0^\infty d\nu B(\mathbf{q}, \nu) \frac{2\nu}{(i\nu_n)^2 - \nu^2}$$

phonon spectral function

$$B(\mathbf{q}, \nu) \equiv -\frac{1}{\pi} \mathrm{Im} D(\mathbf{q}, \nu + i\delta).$$

Normal state

$$\Sigma(\mathbf{k}, i\omega_m) = \frac{1}{N\beta} \sum_{\mathbf{k}', m'} \int_0^\infty d\nu |g_{\mathbf{k},\mathbf{k}'}|^2 B(\mathbf{k} - \mathbf{k}', \nu) \frac{2\nu}{(\omega_m - \omega_{m'})^2 + \nu^2} G_\circ(\mathbf{k}', i\omega_{m'}).$$

form of Eq. (15) allows one to introduce the electron-phonon spectral function,

$$\alpha^2 F(\mathbf{k}, \mathbf{k}', \nu) \equiv N(\mu) |g_{\mathbf{k},\mathbf{k}'}|^2 B(\mathbf{k} - \mathbf{k}', \nu),$$

$$\frac{1}{N}\sum_{\mathbf{k}} \rightarrow \int d\epsilon N(\epsilon) \tag{18}$$

along with a constant density of states approximation, extended over an infinite bandwidth, one obtains for the electron self energy

$$\Sigma(i\omega_m) = \lambda\omega_E^2 \int_{-\infty}^{\infty} d\epsilon \frac{1}{\beta}\sum_{m'} \frac{1}{\omega_E^2 + (\omega_{m'} - \omega_m)^2} \frac{1}{i\omega_{m'} - (\epsilon - \mu)}, \tag{19}$$

where we have used the standard definition for the electron-phonon mass enhancement parameter, λ:

$$\lambda \equiv 2\int_0^{\infty} d\nu \frac{\alpha^2 F(\nu)}{\nu}, \tag{20}$$

which, for the Einstein spectrum used here, reduces to

$$\lambda = 2N(\epsilon_F)g^2/\omega_E. \tag{21}$$

Performing the Matsubara sum yields

$$\Sigma(i\omega_m) = \frac{\lambda\omega_E}{2}\int_{-\infty}^{\infty} d\epsilon \Big(\frac{n(\omega_E) + 1 - f(\epsilon - \mu)}{i\omega_m - \omega_E - (\epsilon - \mu)} + \frac{n(\omega_E) + f(\epsilon - \mu)}{i\omega_m + \omega_E - (\epsilon - \mu)} \Big) \tag{22}$$

where $f(\epsilon - \mu)$ is the Fermi function and $n(\omega_E)$ is the Bose distribution function. The remaining integral can also be performed [13]

$$\Sigma(z) = \frac{\lambda\omega_E}{2}\Big[-2\pi i(n(\omega_E) + 1/2) + \psi(\frac{1}{2} + i\frac{\omega_E - z}{2\pi T}) - \psi(\frac{1}{2} - i\frac{\omega_E + z}{2\pi T}) \Big] \tag{23}$$

where $\psi(x)$ is the digamma function [92, 13] and the entire expression has been analytically continued to a general complex frequency z. Because we performed the Matsubara sum first, before replacing $i\omega_m$ with z, this is the physically correct analytic continuation [93].

is the Heaviside step function), the self energy at $T = 0$ is

$$\Sigma(z) = \frac{\lambda\omega_E}{2} \ln\left(\frac{\omega_E - z}{\omega_E + z}\right). \tag{24}$$

Spectroscopic measurements yield properties as a function of real frequency; because of the analytic properties of the Green function, this corresponds to a frequency either slightly above or below the real axis. We will use frequencies slightly above, and designate the infinitesmal positive imaginary part by '$i\delta$'. Thus,

$$\Sigma(\omega + i\delta) = \frac{\lambda\omega_E}{2}\left[\ln \mid \frac{\omega_E - \omega}{\omega_E + \omega} \mid -i\pi\theta(\mid \omega \mid -\omega_E)\right]. \tag{25}$$

The real and imaginary parts of this self energy are shown in Fig. 3, along with the non-interacting inverse Green function $(\omega - (\epsilon_{\mathbf{k}} - \mu))$ to determine the poles of the electron Green function (see Eq. (6)) graphically. A quantity often measured in single particle spectroscopies is the spectral function, $A(\mathbf{k}, \omega)$ defined by

$$A(\mathbf{k}, \omega) \equiv -\frac{1}{\pi}\mathrm{Im}G(\mathbf{k}, \omega + i\delta). \tag{26}$$

With this definition, we obtain, through Eq. (6) and (25),

$$\begin{aligned} A(\mathbf{k}, \omega) &= \delta\left(\omega - (\epsilon_{\mathbf{k}} - \mu) - \frac{\lambda\omega_E}{2} \ln \mid \frac{\omega_E - \omega}{\omega_E + \omega} \mid\right) && \text{if } \mid \omega \mid < \omega_E, \\ &= \frac{\lambda\omega_E/2}{\left(\omega - (\epsilon_{\mathbf{k}} - \mu) - \frac{\lambda\omega_E}{2} \ln \mid \frac{\omega_E - \omega}{\omega_E + \omega} \mid\right)^2 + \left(\frac{\pi\lambda\omega_E}{2}\right)^2} && \text{if } \mid \omega \mid > \omega_E. \end{aligned} \tag{27}$$

Plots are shown in Fig. 4. Each spectral function displays a quasiparticle peak, whose strength $a_{\mathbf{k}}$ and frequency $\omega_{\mathbf{k}}$ is implicitly dependent on wavevector

$$a_{\mathbf{k}} = \left(1 + \frac{\lambda}{1 - (\omega_{\mathbf{k}}/\omega_E)^2}\right)^{-1}, \tag{28}$$

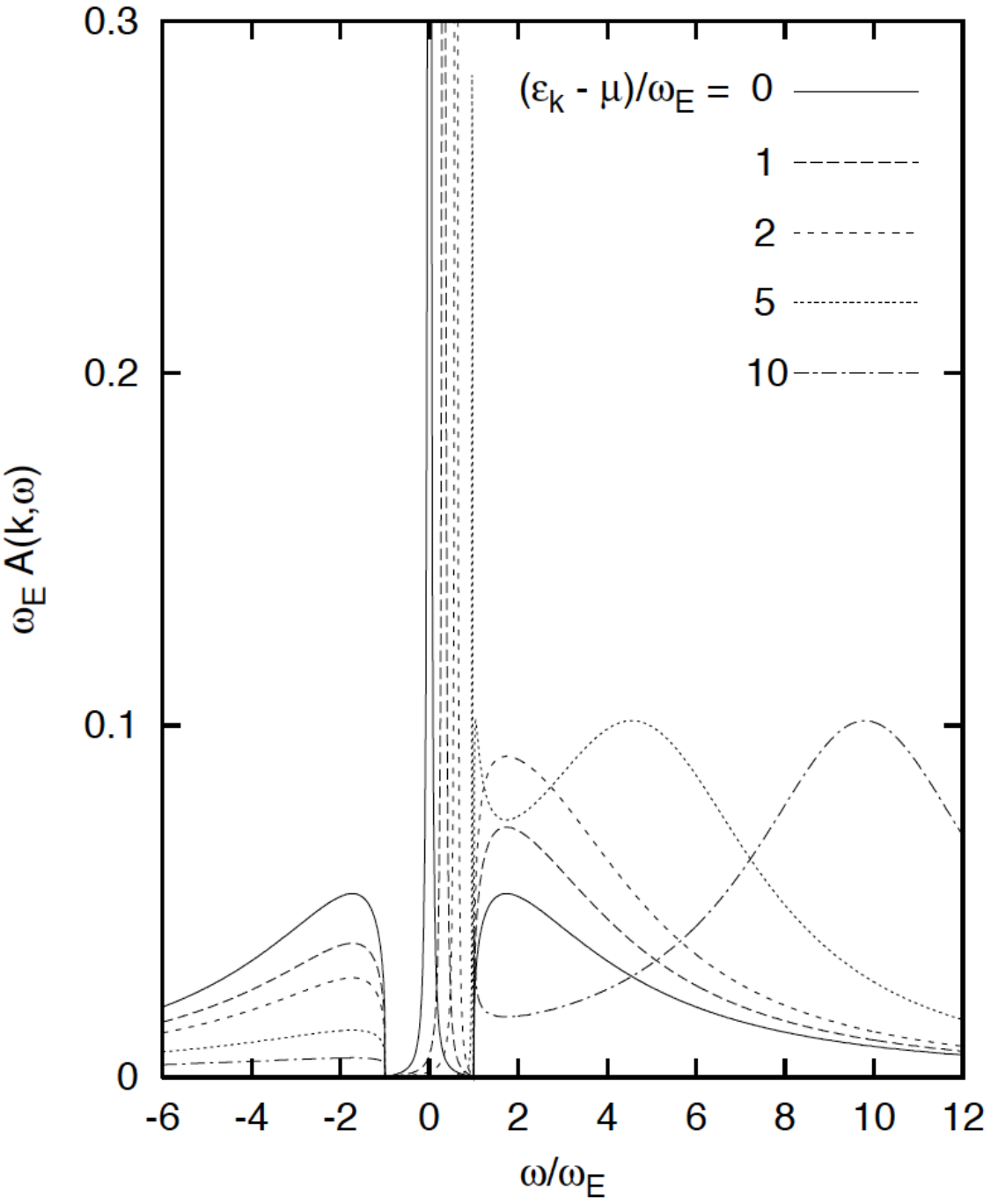
0.3
0.2
0.1
0
-6
-4
-2
0
2
4
6
8
10
12
$\omega_E A(k,\omega)$
ω/ω_E
$(\varepsilon_k - \mu)/\omega_E =$ 0
1
2
5
10

phonons

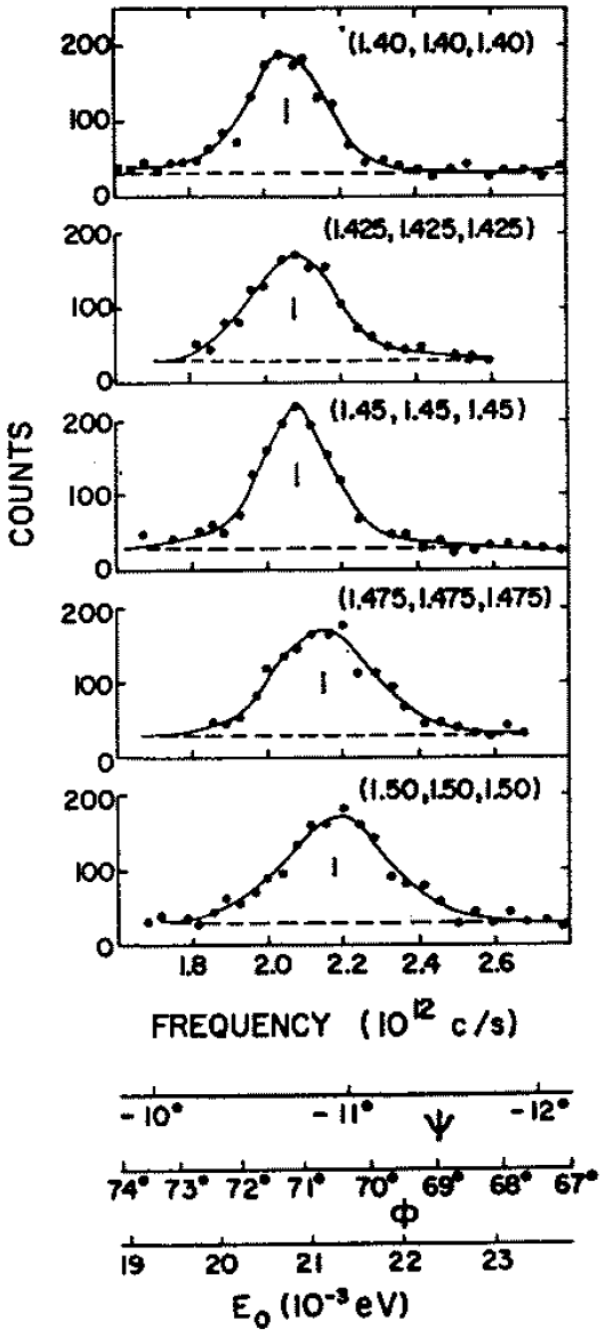
(1.40, 1.40, 1.40)
(1.425, 1.425, 1.425)
(1.45, 1.45, 1.45)
(1.475, 1.475, 1.475)
(1.50, 1.50, 1.50)
COUNTS
FREQUENCY (10^12 c/s)
Ψ
Φ
E0 (10^-3 eV)

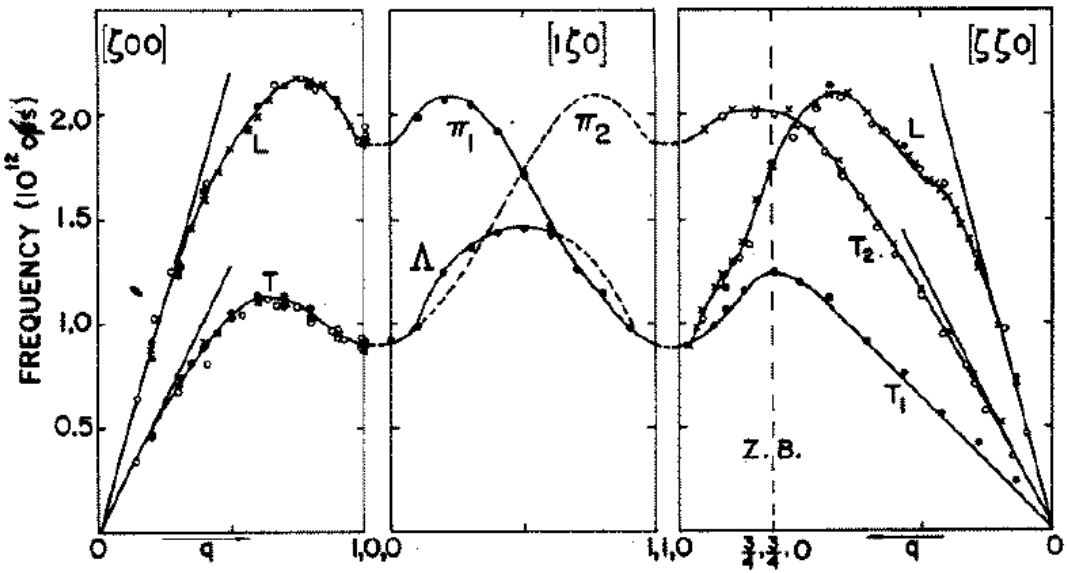
[ζ00]
[1ζ0]
[ζζ0]
FREQUENCY (10^12 cps)
L
T
Λ
Z. B.

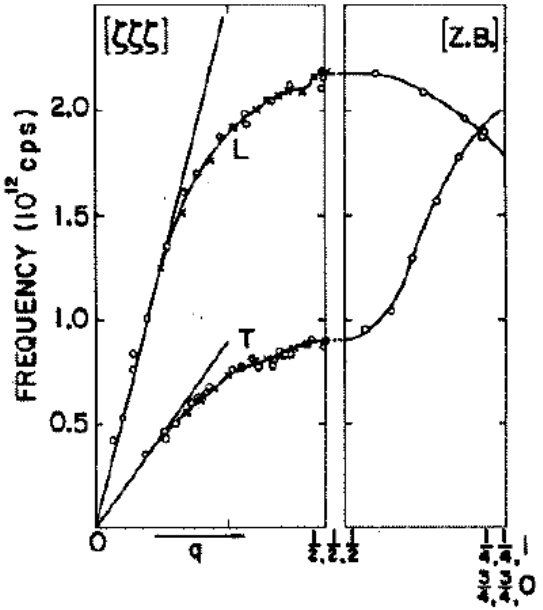
[ζζζ]
[Z.B.]
FREQUENCY (10^12 cps)
L
T

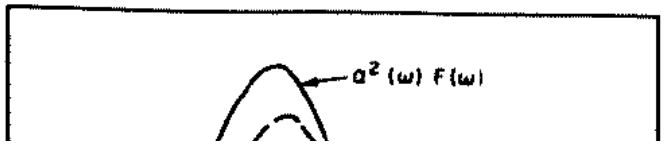

Recall:

$$\Sigma(\mathbf{k}, i\omega_m) = \frac{1}{N\beta}\sum_{\mathbf{k}',m'}\int_0^\infty d\nu |g_{\mathbf{k},\mathbf{k}'}|^2 B(\mathbf{k}-\mathbf{k}',\nu)\frac{2\nu}{(\omega_m-\omega_{m'})^2+\nu^2}G_\circ(\mathbf{k}', i\omega_{m'}).$$

form of Eq. (15) allows one to introduce the electron-phonon spectral function,

$$\alpha^2 F(\mathbf{k},\mathbf{k}',\nu) \equiv N(\mu)|g_{\mathbf{k},\mathbf{k}'}|^2 B(\mathbf{k}-\mathbf{k}',\nu),$$

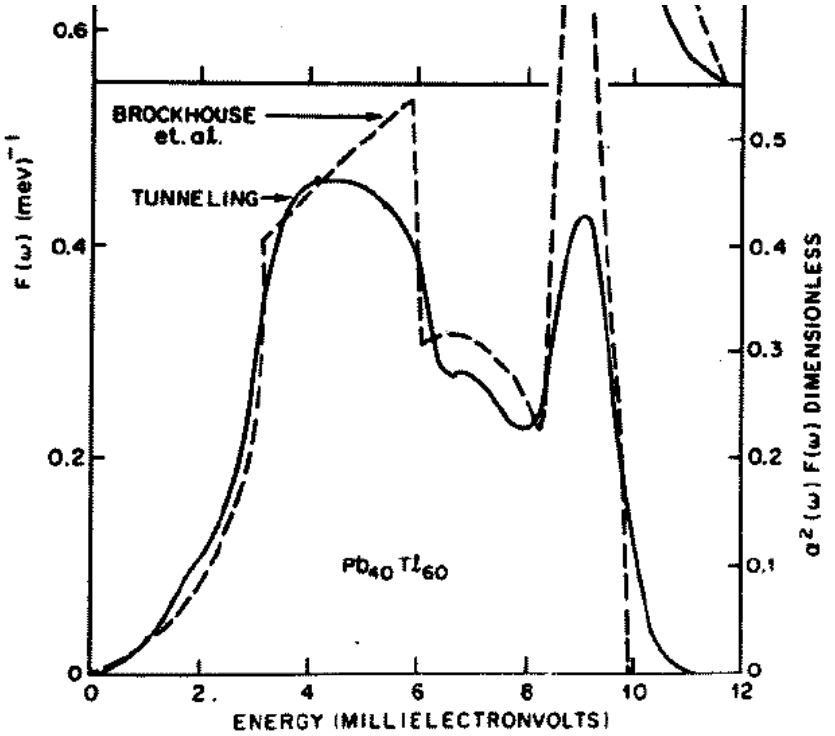

Recall:

$$\Sigma(\mathbf{k}, i\omega_m) \equiv \frac{1}{N\beta} \sum_{\mathbf{k}',m'} \frac{\lambda_{\mathbf{k}\mathbf{k}'}(i\omega_m - i\omega_{m'})}{N(\mu)} G(\mathbf{k}', i\omega_{m'}) \tag{42}$$

$$\phi(\mathbf{k}, i\omega_m) \equiv \frac{1}{N\beta} \sum_{\mathbf{k}',m'} \left[\frac{\lambda_{\mathbf{k}\mathbf{k}'}(i\omega_m - i\omega_{m'})}{N(\mu)} - V_{\mathbf{k}\mathbf{k}'} \right] F(\mathbf{k}', i\omega_{m'}), \tag{43}$$

$$G(\mathbf{k}, i\omega_m) = \frac{G_n^{-1}(\mathbf{k}, i\omega_m)}{G_n^{-1}(\mathbf{k}, i\omega_m) G_n^{-1}(-\mathbf{k}, -i\omega_m) + \phi(\mathbf{k}, i\omega_m)\bar{\phi}(\mathbf{k}, i\omega_m)} \tag{44}$$

$$F(\mathbf{k}, i\omega_m) = \frac{\phi(\mathbf{k}, i\omega_m)}{G_n^{-1}(\mathbf{k}, i\omega_m) G_n^{-1}(-\mathbf{k}, -i\omega_m) + \phi(-\mathbf{k}, -i\omega_m)\bar{\phi}(-\mathbf{k}, -i\omega_m)} \tag{45}$$

$$G_n^{-1}(\mathbf{k}, i\omega_m) = G_\circ^{-1}(\mathbf{k}, i\omega_m) - \Sigma(\mathbf{k}, i\omega_m). \tag{46}$$

Use:

$$i\omega_m[1 - Z(\mathbf{k}, i\omega_m)] \equiv \frac{1}{2}[\Sigma(\mathbf{k}, i\omega_m) - \Sigma(\mathbf{k}, -i\omega_m)]$$

$$\chi(\mathbf{k}, i\omega_m) \equiv \frac{1}{2}[\Sigma(\mathbf{k}, i\omega_m) + \Sigma(\mathbf{k}, -i\omega_m)]$$

$$Z(\mathbf{k}, i\omega_m) = 1 + \frac{1}{N\beta}\sum_{\mathbf{k}',m'} \frac{\lambda_{\mathbf{k}\mathbf{k}'}(i\omega_m - i\omega_{m'})}{N(\mu)} \frac{(\omega_{m'}/\omega_m) Z(\mathbf{k}', i\omega_{m'})}{\omega_{m'}^2 Z^2(\mathbf{k}', i\omega_{m'}) + (\epsilon_{\mathbf{k}'} - \mu + \chi(\mathbf{k}', i\omega_{m'}))^2 + \phi^2(\mathbf{k}', i\omega_{m'})} \quad (49)$$

$$\chi(\mathbf{k}, i\omega_m) = -\frac{1}{N\beta}\sum_{\mathbf{k}',m'} \frac{\lambda_{\mathbf{k}\mathbf{k}'}(i\omega_m - i\omega_{m'})}{N(\mu)} \frac{\epsilon_{\mathbf{k}'} - \mu + \chi(\mathbf{k}', i\omega_{m'})}{\omega_{m'}^2 Z^2(\mathbf{k}', i\omega_{m'}) + (\epsilon_{\mathbf{k}'} - \mu + \chi(\mathbf{k}', i\omega_{m'}))^2 + \phi^2(\mathbf{k}', i\omega_{m'})} \quad (50)$$

along with the gap equation (Eq. (43)):

$$\phi(\mathbf{k}, i\omega_m) = \frac{1}{N\beta}\sum_{\mathbf{k}',m'} \left(\frac{\lambda_{\mathbf{k}\mathbf{k}'}(i\omega_m - i\omega_{m'})}{N(\mu)} - V_{\mathbf{k}\mathbf{k}'} \right) \frac{\phi(\mathbf{k}', i\omega_{m'})}{\omega_{m'}^2 Z^2(\mathbf{k}', i\omega_{m'}) + (\epsilon_{\mathbf{k}'} - \mu + \chi(\mathbf{k}', i\omega_{m'}))^2 + \phi^2(\mathbf{k}', i\omega_{m'})}. \quad (51)$$

Simplifications (ignore momentum dependence) give rise to:

along with :

$$Z_m = 1 + \pi T \sum_{m'} \lambda(i\omega_m - i\omega_{m'}) \frac{(\omega_{m'}/\omega_m) Z_{m'}}{\sqrt{\omega_{m'}^2 Z_{m'}^2 + \phi_{m'}^2}} A_0(m') \quad (54)$$

$$\chi_m = -\pi T \sum_{m'} \lambda(i\omega_m - i\omega_{m'}) A_1(m') \quad (55)$$

$$\phi_m = \pi T \sum_{m'} \left(\lambda(i\omega_m - i\omega_{m'}) - N(\mu) V_{\text{coul}} \right) \frac{\phi_{m'}}{\sqrt{\omega_{m'}^2 Z_{m'}^2 + \phi_{m'}^2}} A_0(m') \quad (56)$$

$$n = 1 - 2\pi T N(\mu) \sum_{m'} A_1(m') \quad (57)$$

then, with the additional approximation of infinite bandwidth, $A_0(m') \equiv 1$ (actually a cutoff, $\theta(\omega_c - |\,\omega_{m'}\,|)$, is required in Eq. (56)), and $A_1(m') \equiv 0$. This last result effectively removes χ_m (and Eqs. (55,57)) from further consideration. An earlier review by one of us [11]

3.3 Extraction from Experiment

of the function $\alpha^2 F(\nu)$

$$G(\mathbf{k}, i\omega_m) = \int_{-\infty}^{\infty} d\omega \, \frac{A(\mathbf{k}, \omega)}{i\omega_m - \omega}$$

$$F(\mathbf{k}, i\omega_m) = \int_{-\infty}^{\infty} d\omega \, \frac{C(\mathbf{k}, \omega)}{i\omega_m - \omega},$$

Eq. (26) and $C(\mathbf{k}, \omega)$ is given by a simil

$$C(\mathbf{k}, \omega) \equiv -\frac{1}{\pi} \mathrm{Im} F(\mathbf{k}, \omega + i\delta).$$

$Z(\omega + i\delta) = 1 + \frac{i\pi T}{\omega} \sum^{\infty}$

3.3.2 Tunneling

$$I_S(V) \propto \int d\omega \mathrm{Re}\left[\frac{|\omega|}{\sqrt{\omega^2 - \Delta^2(\omega)}}\right][f(\omega) - f(\omega + V)], \quad (73)$$

$\phi(\omega$ used the gap function, $\Delta(\omega)$, defined as

$$\Delta(\omega) \equiv \phi(\omega + i\delta)/Z(\omega + i\delta).$$

ality constant contains information about the density of state
eptor), and the tunneling matrix element. These are usuall (74)
e takes the zero temperature limit, then the derivative of t
oltage is simply proportional to the superconducting densit

$$\left(\frac{dI}{dV}\right)_S \Big/ \left(\frac{dI}{dV}\right)_N = \mathrm{Re}\left(\frac{|V|}{\sqrt{V^2 - \Delta^2(V)}}\right),$$

BCS formalism vs. Pairing Mechanism

$$\Delta = |V| \frac{1}{N} \sum_k \frac{\Delta}{2E_k}$$

Tc equation (useless)

$$\frac{2\Delta}{k_B T_c} = 3.53$$

Universality

$$\frac{\Delta C}{\gamma T_c} = 1.43$$

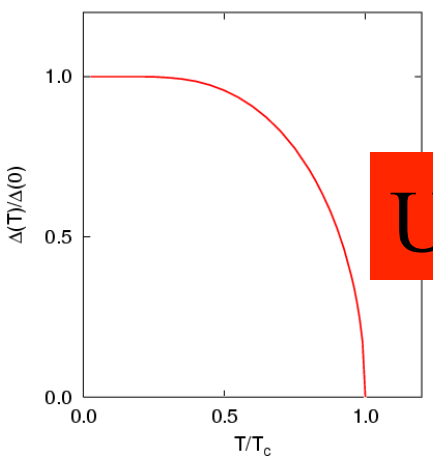

Universality is wonderful

Universality is a curse!

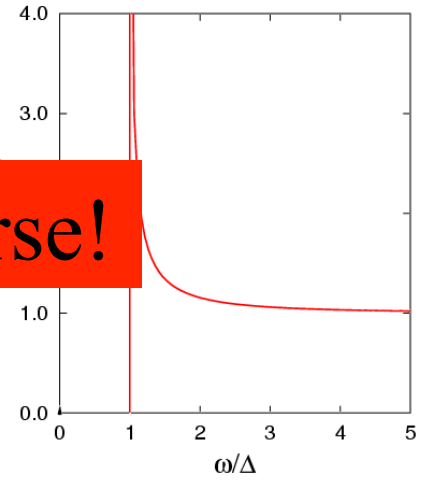

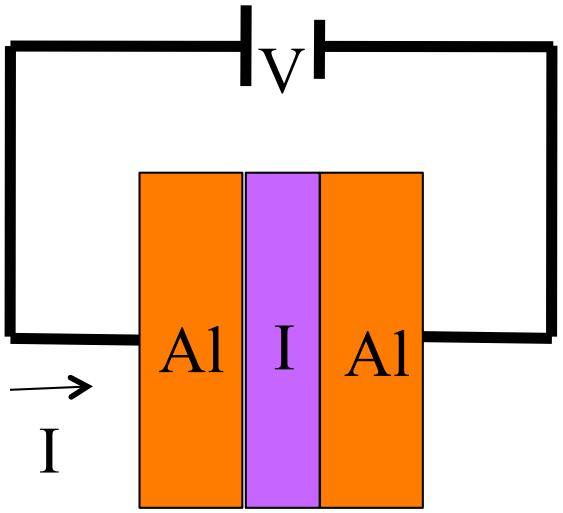

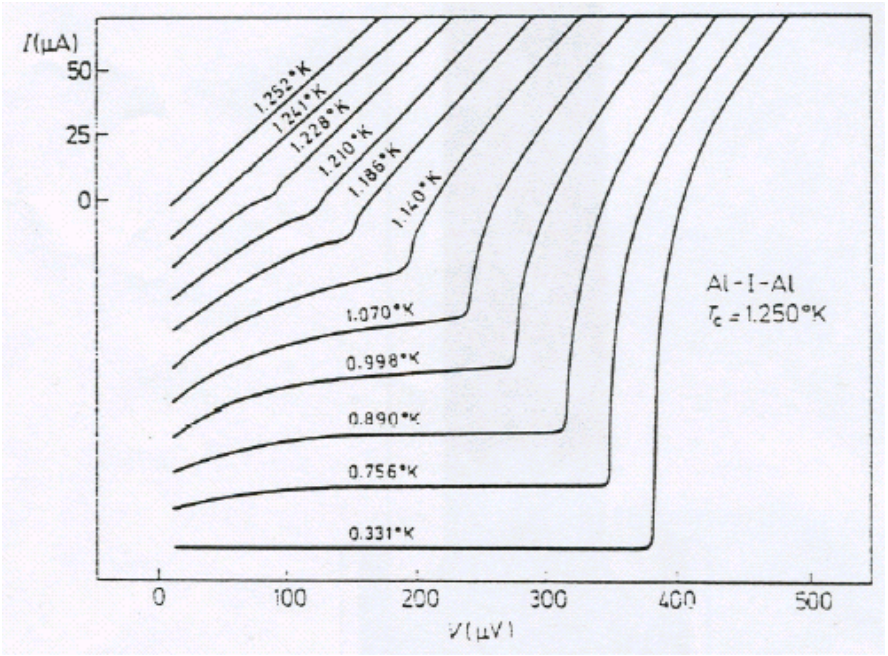

B.L. Blackford and R.H. March, Can. J. Phys. 46, 141 (1968)

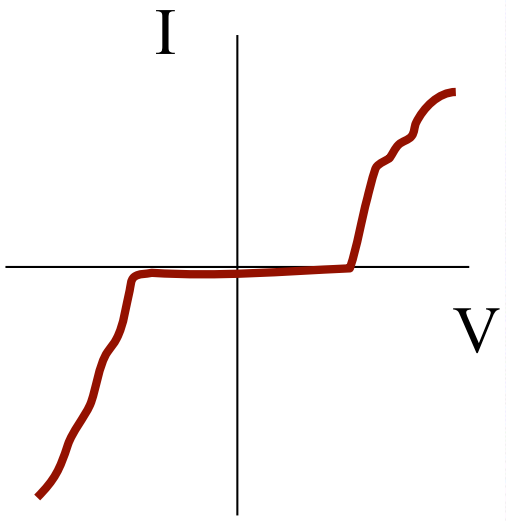

$$\frac{dI}{dV} \propto N(V)$$

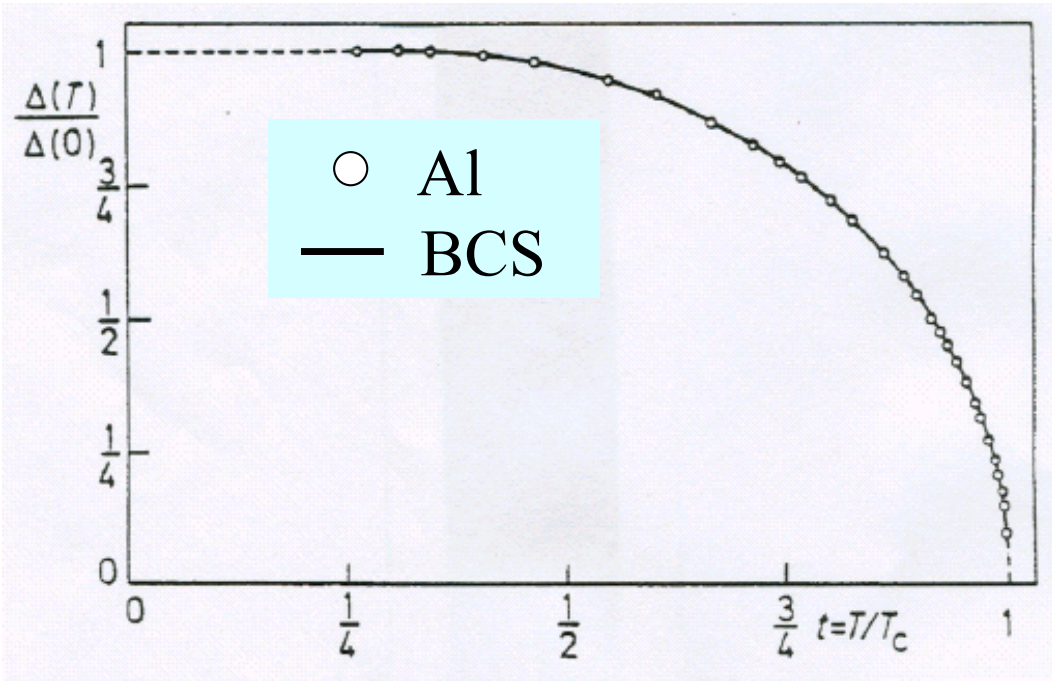

3.3.2 Tunneling

$$I_S(V) \propto \int d\omega \mathrm{Re}\left[\frac{|\omega|}{\sqrt{\omega^2 - \Delta^2(\omega)}}\right][f(\omega) - f(\omega + V)],$$

ıused the gap function, $\Delta(\omega)$, defined as

$$\Delta(\omega) \equiv \phi(\omega + i\delta)/Z(\omega + i\delta).$$

ality constant contains information about the density of state
eptor), and the tunneling matrix element. These are usuall
e takes the zero temperature limit, then the derivative of t
oltage is simply proportional to the superconducting densit

$$\left(\frac{dI}{dV}\right)_S / \left(\frac{dI}{dV}\right)_N = \mathrm{Re}\left(\frac{|V|}{\sqrt{V^2 - \Delta^2(V)}}\right),$$

I. Giaever, H.R. Hart, Jr., and K. Megerle, PRB 126, 941 (1962)

$$\frac{dI}{dV} \sim N(\varepsilon)$$

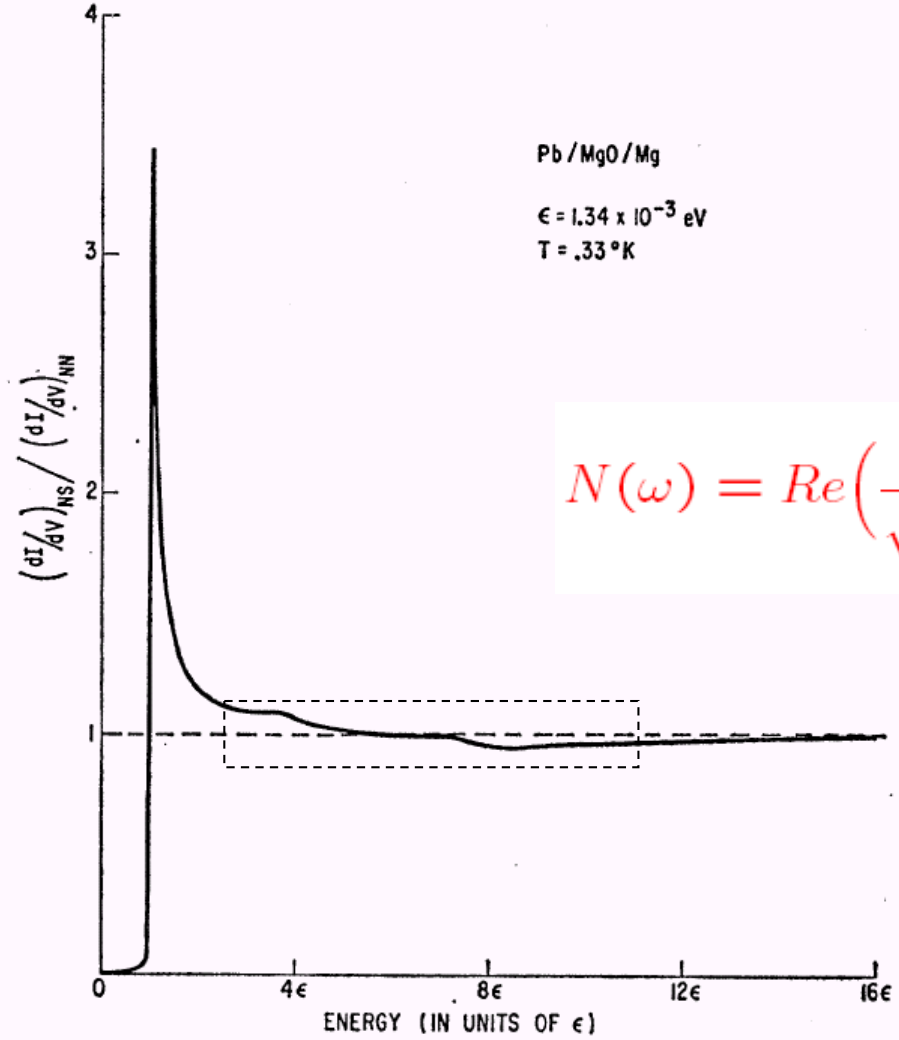

$$N(\omega) = Re\left(\frac{\omega}{\sqrt{\omega^2 - \Delta^2(\omega)}}\right)$$

FIG. 10. The relative conductance of a Pb-MgO-Mg sandwich plotted against energy. At higher energies there are definite divergences from the BCS density of states as can be seen from the bumps in the experimental curve. Note that the crossover point corresponds in energy to the Debye temperature.

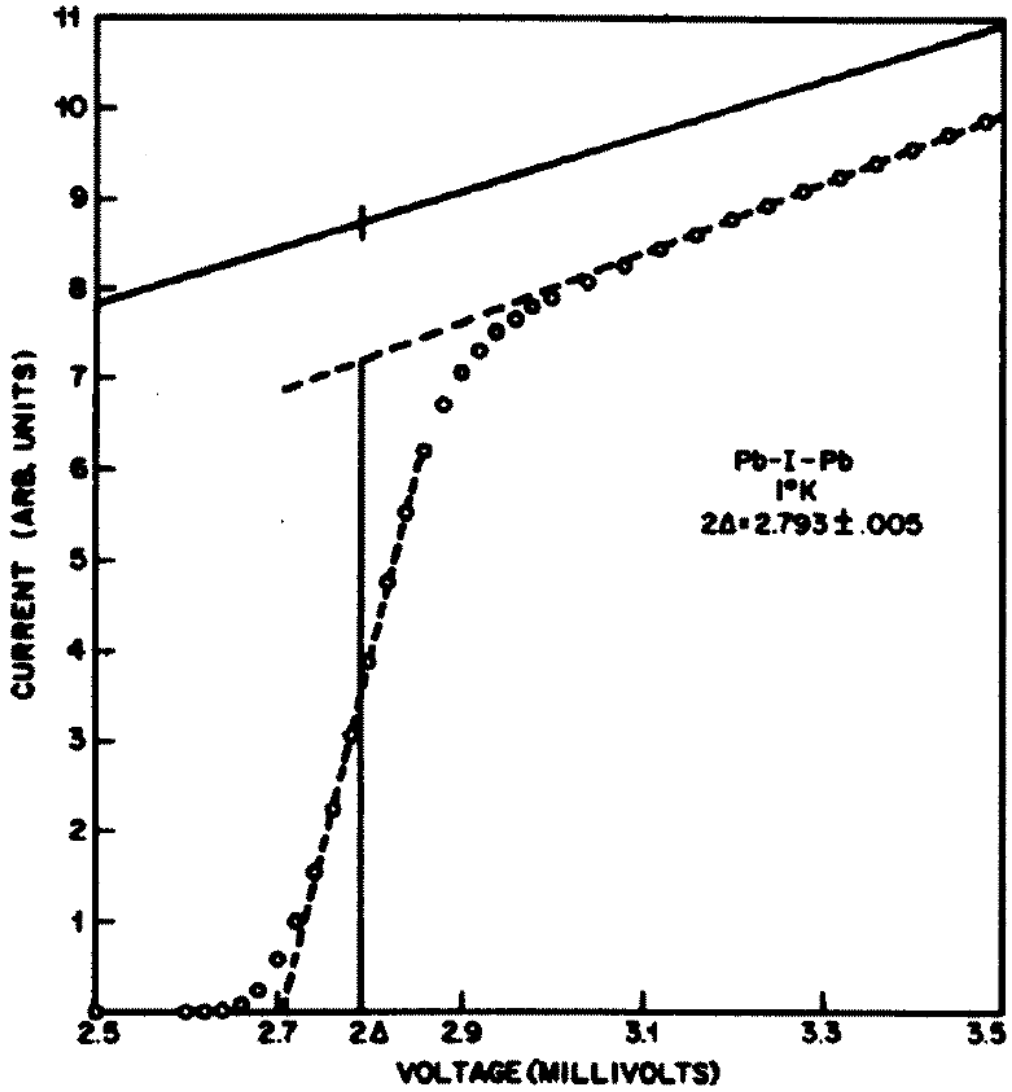

Figure 12: I-V characteristic of a Pb-I-Pb junction showing the construction used to find the energy gap. The solid line and open circles are the current in the normal and superconducting states, respectively. Reproduced from Ref. [52].

Eliashberg Theory

$$\Delta(k,\omega) = \mathcal{F}[V_{k,k'}(\omega,\omega')]$$

$$\downarrow$$

A functional of the interaction

Question: Can we invert the theory to extract the potential uniquely from a knowledge of $\Delta(k,\omega)$?

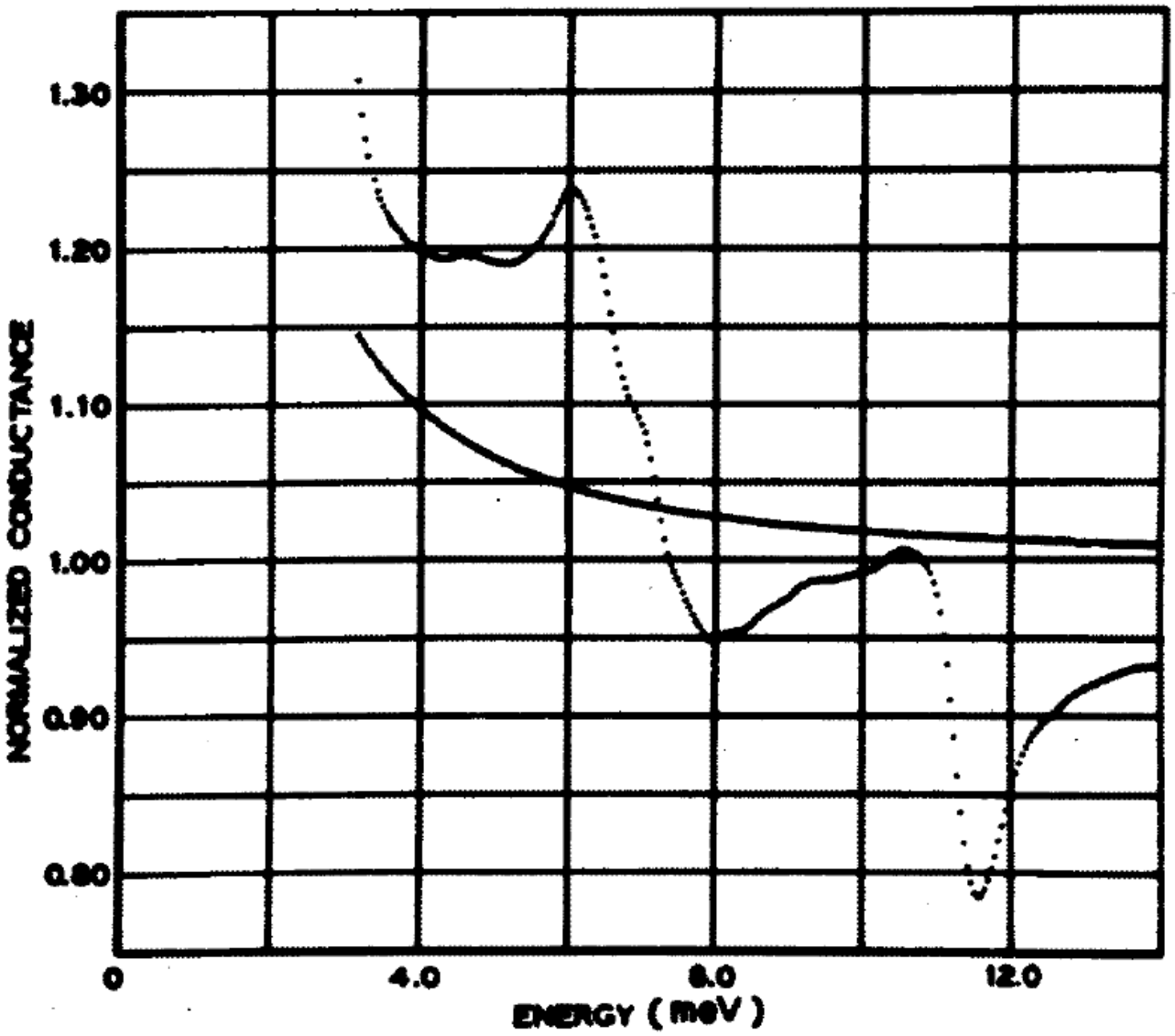

Figure 13: Conductance dI/dV of a Pb-I-Pb junction in the superconducting state normalized by the conductance in the normal state vs. voltage. Also shown is the two-superconductor conductance calculated from the BCS density of states which contains no phonon structure. Reproduced from Ref. [52].

McMillan and Rowell, Superconductivity, ed. By R.D. Parks (1969)

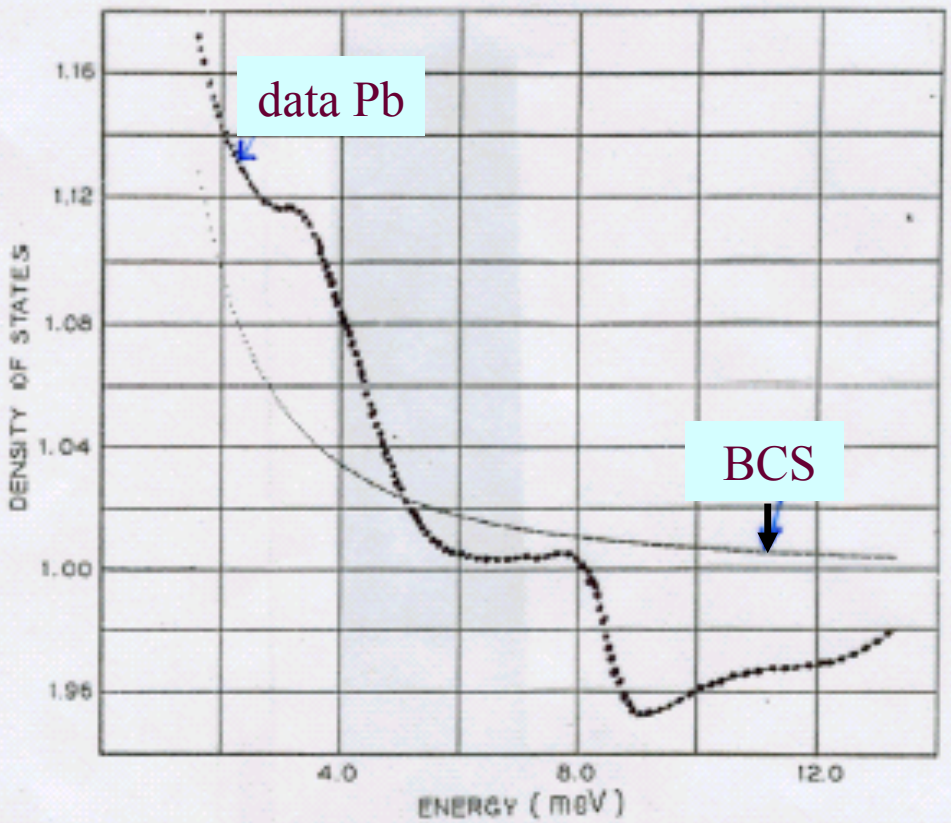

Fig. 23. Electronic density of states $N(E)$ for lead vs. $E-\Delta_0$ obtained from the data of Fig. 19. The smooth curve is the BCS density of states.

requires Eliashberg theory:

- phonon dynamics (retardation) taken into account $[\alpha^2 F(\Omega)]$
  - gap is a function of frequency $\Delta(\omega) = \mathcal{F}[\{\alpha^2 F(\Omega)\}, \mu^*]$
  - density of states is modified: $\frac{dI}{dV} \propto N(\omega) = N(\epsilon_F)\mathrm{Re}\{\frac{\omega}{\sqrt{\omega^2 - \Delta^2(\omega)}}\}$

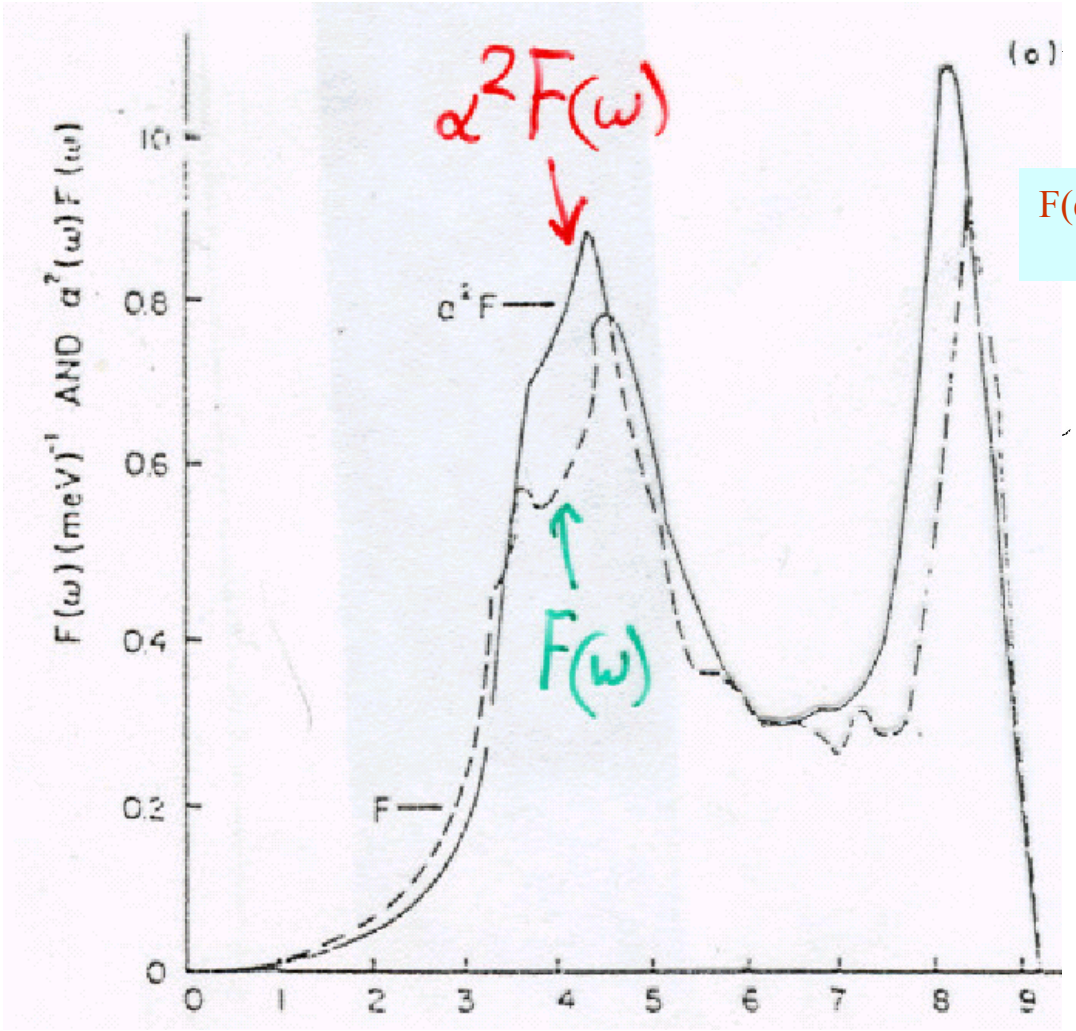

F(ω): density of phonon states from neutron scattering

$$\alpha^2(\omega) \equiv \frac{\alpha^2 F(\omega)}{F(\omega)} \sim \text{constant}$$

McMillan and Rowell, in Superconductivity, ed. By R.D. Parks (1969)

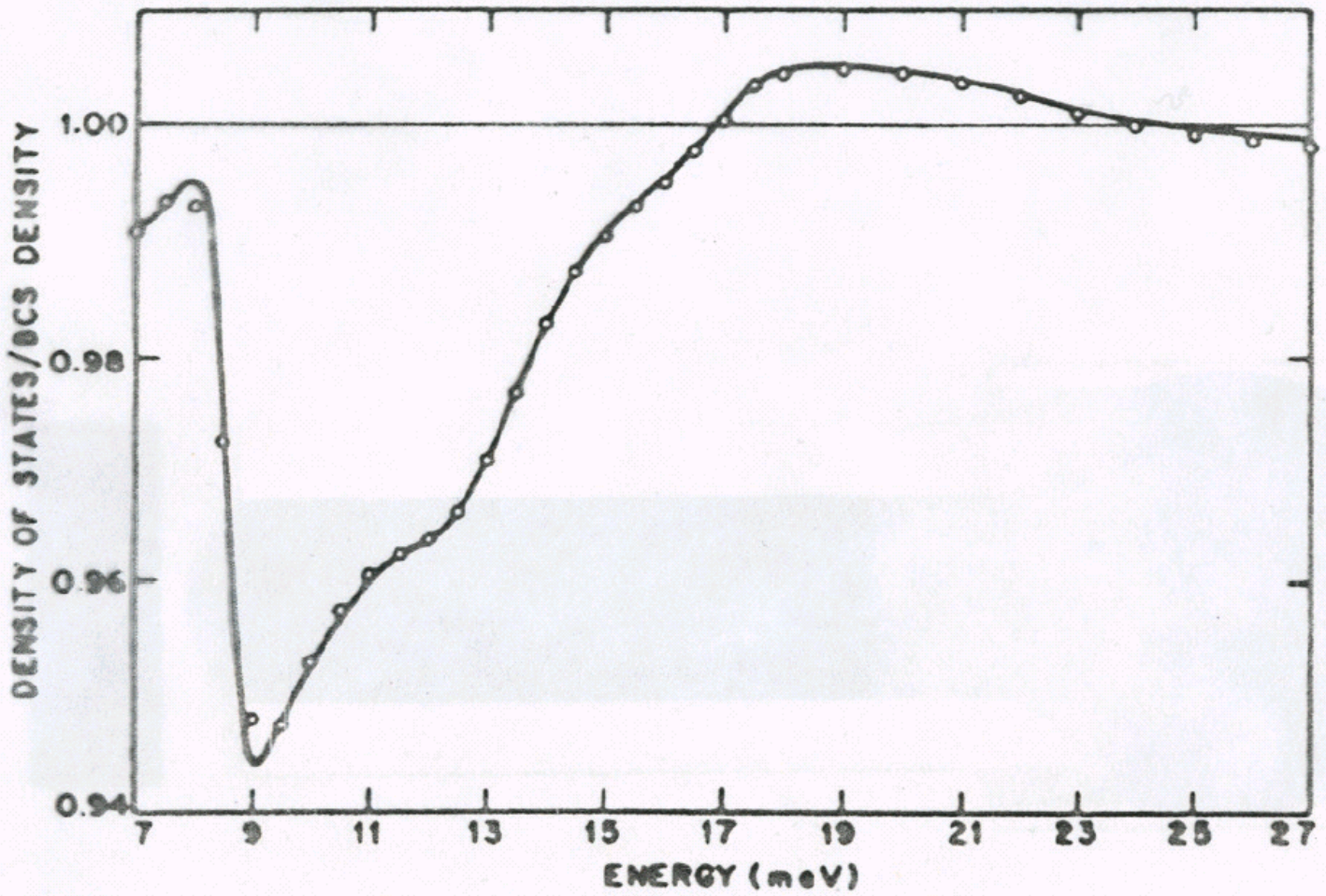

Fig. 32. Calculated (——) and measured (○○○) electronic density of states $N(E)$ for Pb normalized by the BCS density of states vs. $E-\Delta_0$. The measured density of states for $E-\Delta_0 > 11$ meV was not used in the fitting procedure and a comparison of theory and experiment in this "multiple-phonon-emission" region is a valied tst of the theory. In the experiment the sharp drop near 9 meV is affected by thermal smearing.

What does the theory look like?

BCS

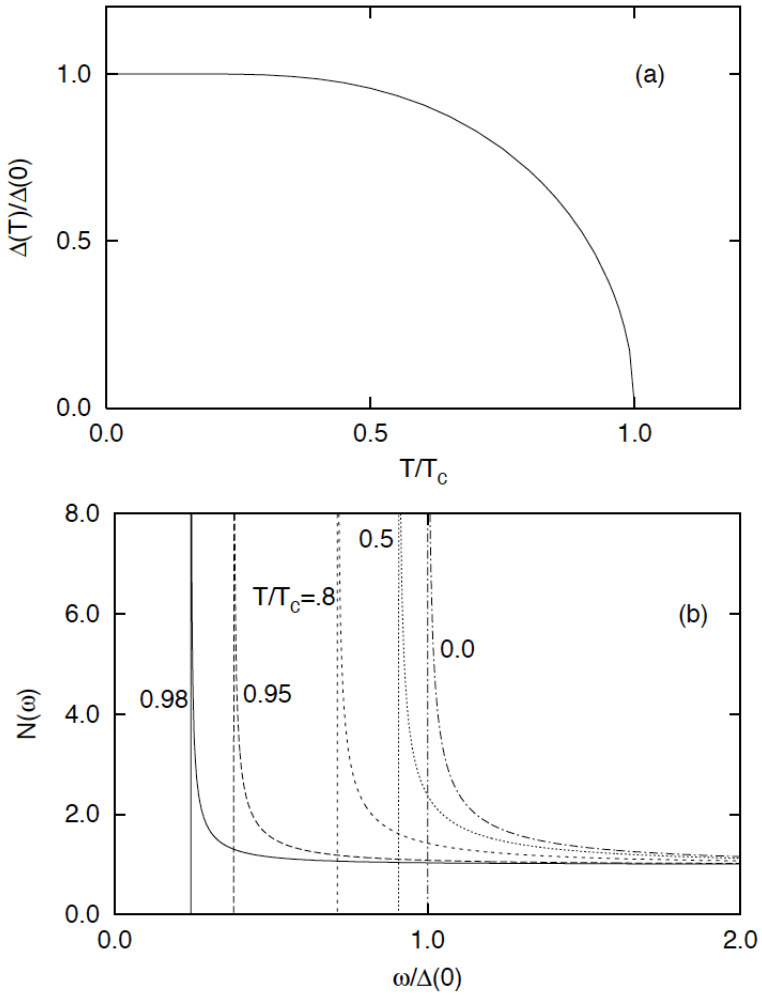

Figure 21: (a) The temperature dependence of the BCS order parameter, and (b) the resulting densities of states at various temperatures below T_c. The only effect of finite temperatures on these latter curves is a reduced gap.

Eliashberg

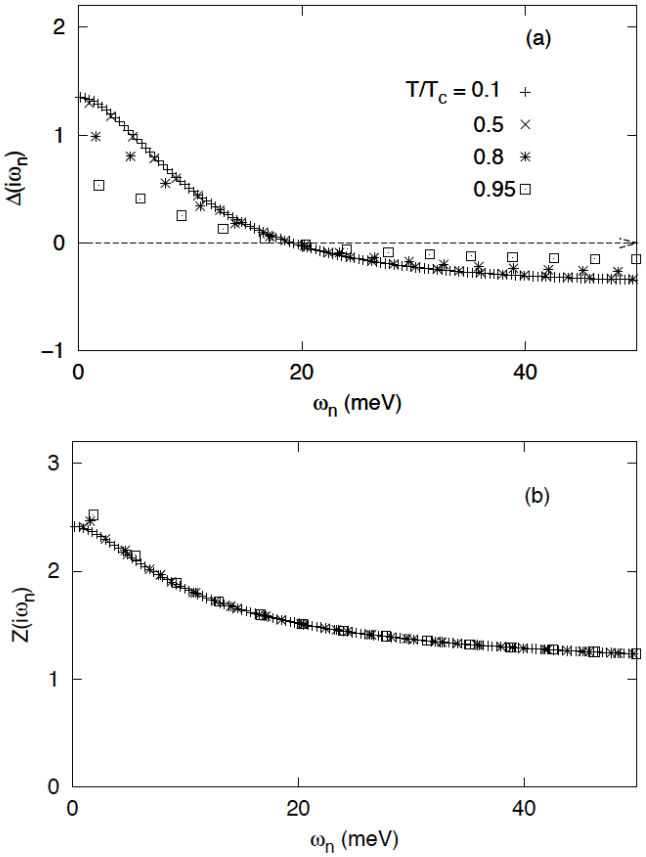

Figure 22: (a) $\Delta(i\omega_n)$ and $Z(i\omega_n)$ vs ω_n, the fermion Matsubara frequency, for various temperatures, as indicated. Note that the curves are relatively smooth and featureless, and at low temperatures little change occurs, except that more Matsubara frequencies are present. In (a) the units of Δ are meV. These were produced for Pb.

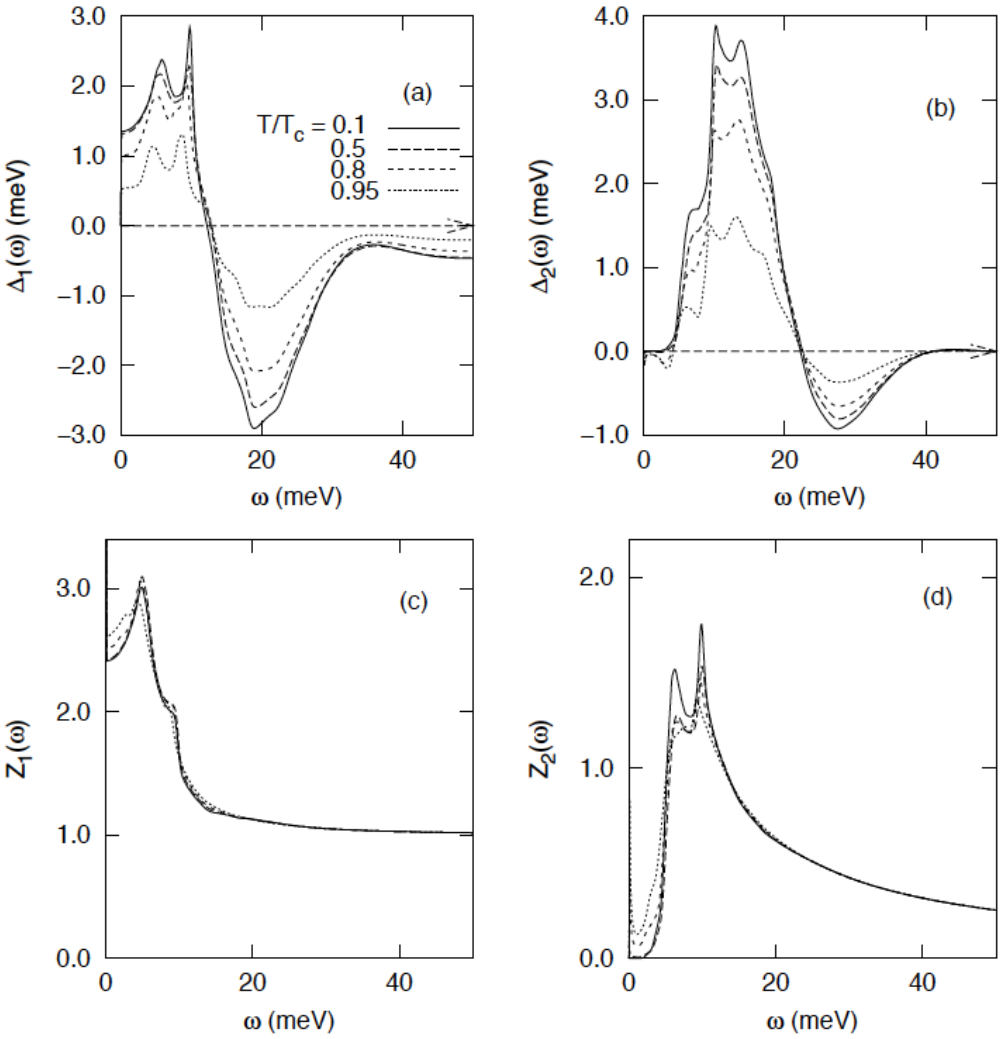

Eliashberg
(real frequency axis)

Figure 23: The (a) real and (b) imaginary parts of the gap function (in meV) on the real frequency axis, for Pb, for various temperatures, as in the previous figure. Note the considerable structure present on the real axis. Also shown is the (c) real and (d) imaginary part of the renormalization function, $Z(\omega)$ vs ω.

Eliashberg Theory

Density of states at finite temperature

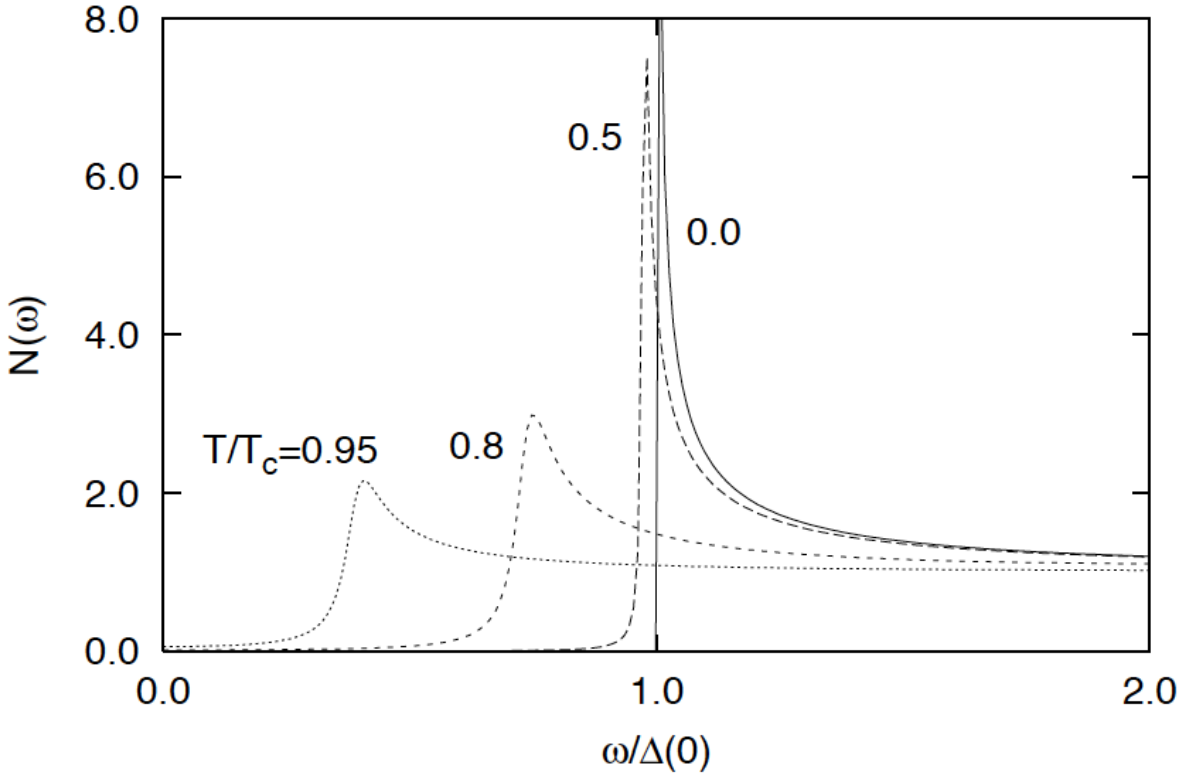

Figure 24: Calculated densities of states of Pb for various temperatures. In contrast to the BCS case (Fig. (21b), at high temperatures there is considerable smearing.

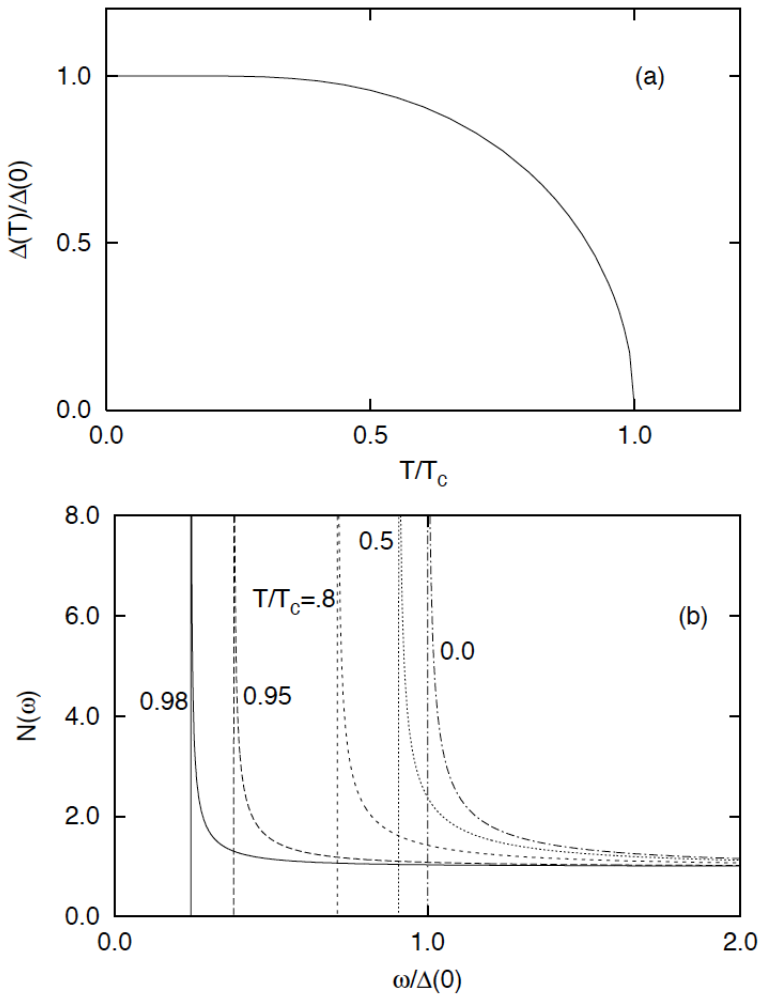

BCS
(at finite temperature)

Figure 21: (a) The temperature dependence of the BCS order parameter, and (b) the resulting densities of states at various temperatures below T_c. The only effect of finite temperatures on these latter curves is a reduced gap.

$$2\Delta_0/k_BT_c = 3.53[1 + 12.5(T_c/\omega_{\ell n})^2 \ell n(\omega_{\ell n}/2T_c)]$$

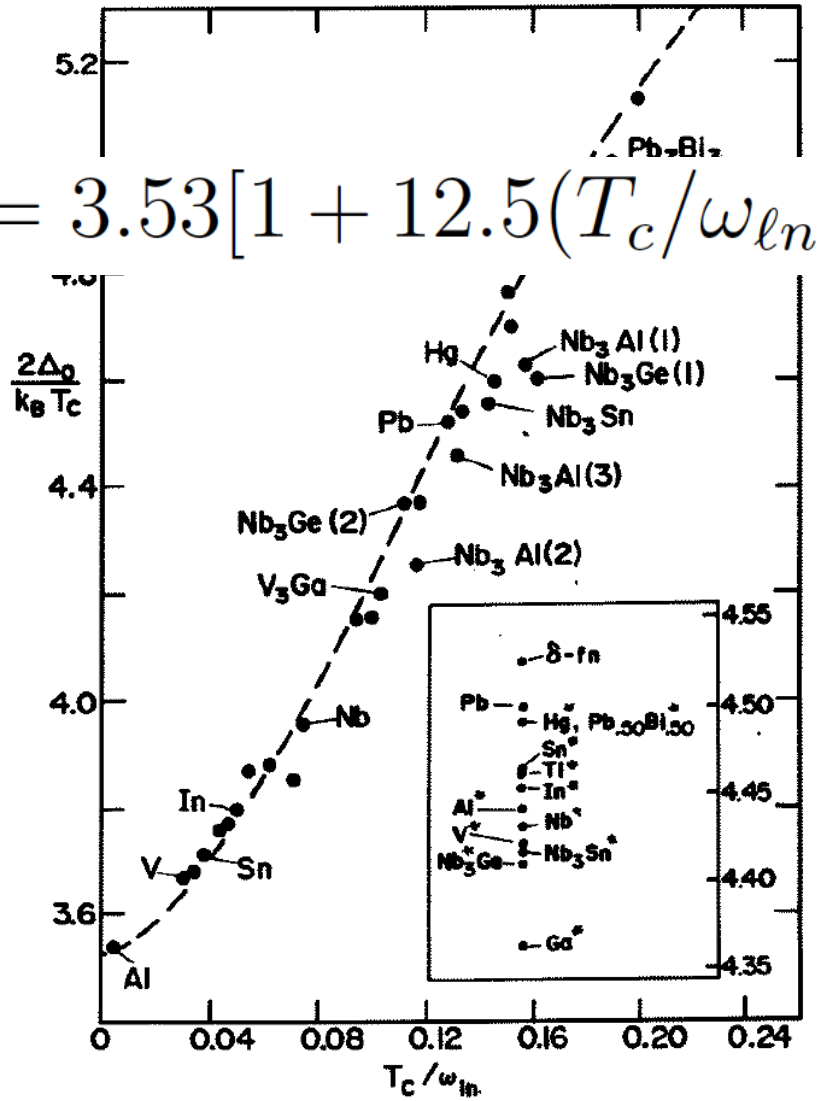

The gap ratio

$$\omega_{\ln} \equiv \exp\left[\frac{2}{\lambda}\int_0^\infty d\nu\, \ln(\nu)\frac{\alpha^2F(\nu)}{\nu}\right].$$

Figure 25: The ratio $2\Delta_0/k_BT_c$ vs $T_c/\omega_{\ell n}$. The solid dots represent results from the full numerical solutions of the Eliashberg equations. Experiment tends to agree to within 10%. In increasing order of $T_c/\omega_{\ell n}$, the dots correspond to the following systems: $A\ell$, V, Ta, Sn, $T\ell$, $T\ell_{0.9}Bi_{0.1}$, In, Nb (Butler), Nb (Arnold), $V_3Si(1)$, V_3Si (Kihl.), Nb (Rowell), Mo, $Pb_{0.4}T\ell_{0.6}$, La, V_3Ga, $Nb_3A\ell(2)$, $Nb_3Ge(2)$, $Pb_{0.6}T\ell_{0.4}$, Pb, $Nb_3A\ell(3)$, $Pb_{0.8}T\ell_{0.2}$, Hg, Nb_3Sn, $Pb_{0.9}Bi_{0.1}$, $Nb_3A\ell(1)$, $Nb_3Ge(1)$, $Pb_{0.8}Bi_{0.2}$, $Pb_{0.7}Bi_{0.3}$, and $Pb_{0.65}Bi_{0.35}$. The drawn curve corresponds to $2\Delta_0/k_BT_c = 3.53[1 + 12.5(T_c/\omega_{\ell n})^2\ell n(\omega_{\ell n}/2T_c)]$. The insert shows results for different scaled $\alpha^2F(\omega)$ spectra. They all correspond to the same value of T_c and of $\omega_{\ell n}$ as Pb. They serve to show that some deviation from the general trend is possible. Reproduced from Ref. [11].

The Specific Heat Jump at Tc

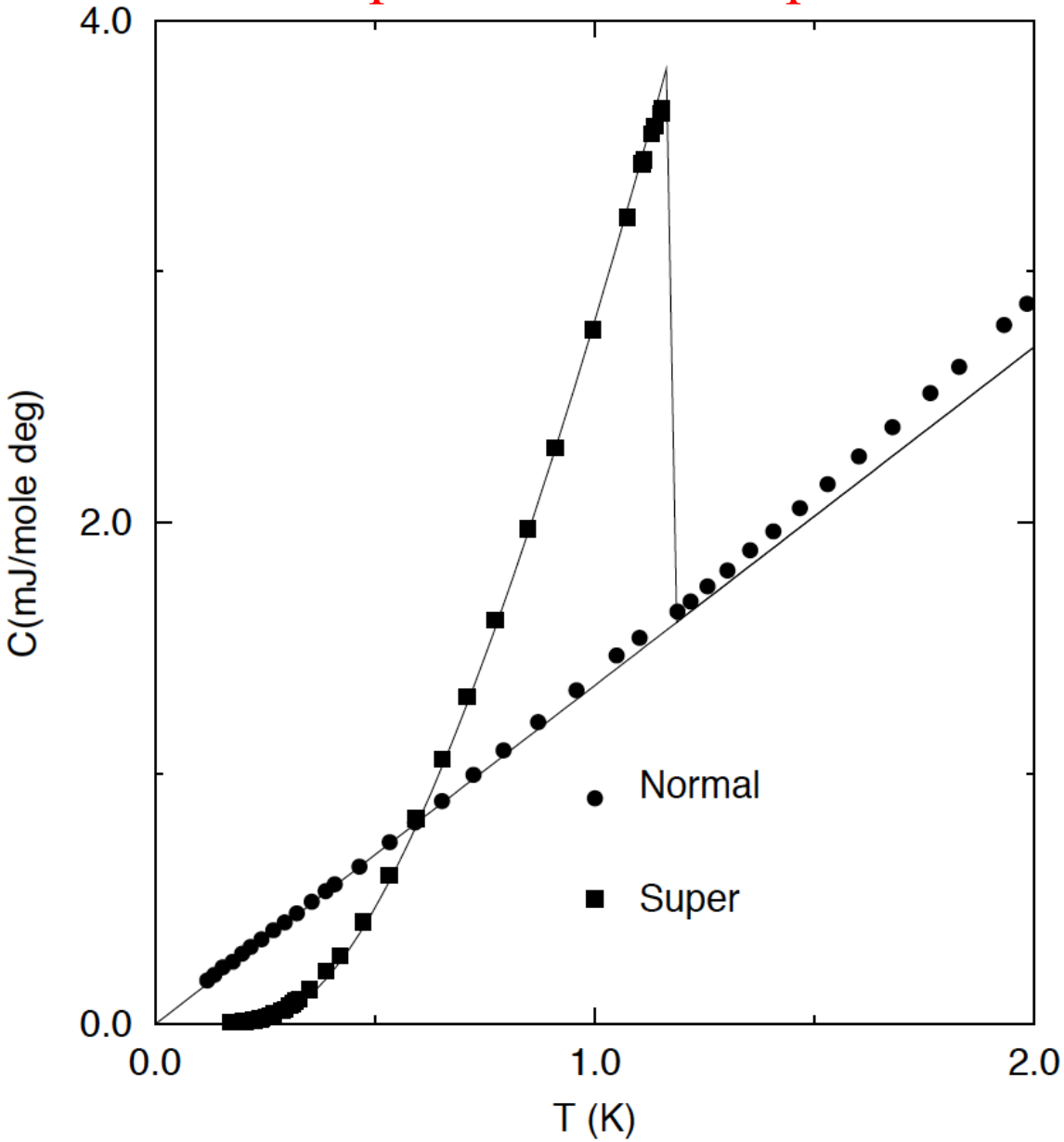

Figure 26: Specific heat of aluminium as a function of temperature in the superconducting state and the normal state (applied field of 300 Gauss). Data taken from Ref. [237]. The BCS prediction, given the normal state data, is given by the solid curve.

Figure 27: The specific heat ratio, $\Delta C(T_c)/(\gamma T_c)$ vs $T_c/\omega_{\ell n}$. The dots represent results from the full numerical solutions of the Eliashberg equations. Experiment tends to agree to within 10%. In increasing order of $T_c/\omega_{\ell n}$, the dots correspond to the following systems: $A\ell$, V, Ta, Sn, $T\ell$, $T\ell_{0.9}Bi_{0.1}$, In, Nb (Butler), Nb (Arnold), V_3Si 1, V_3Si (Kihl.), Nb (Rowell), Mo, $Pb_{0.4}T\ell_{0.6}$, La, V_3Ga, $Nb_3A\ell(2)$, $Nb_3Ge(2)$, $Pb_{0.6}T\ell_{0.4}$, Pb, $Nb_3A\ell(3)$, $Pb_{0.8}T\ell_{0.2}$, Hg, Nb_3Sn, $Pb_{0.9}Bi_{0.1}$, $Nb_3A\ell(1)$, $Nb_3Ge(1)$, $Pb_{0.8}Bi_{0.2}$, $Pb_{0.7}Bi_{0.3}$, and $Pb_{0.65}Bi_{0.35}$. The drawn curve corresponds to $\Delta C(T_c)/\gamma T_c = 1.43(1 + 53(T_c/\omega_{\ell n})^2 \ell n(\omega_{\ell n}/3T_c))$. Adapted from Ref. [221].

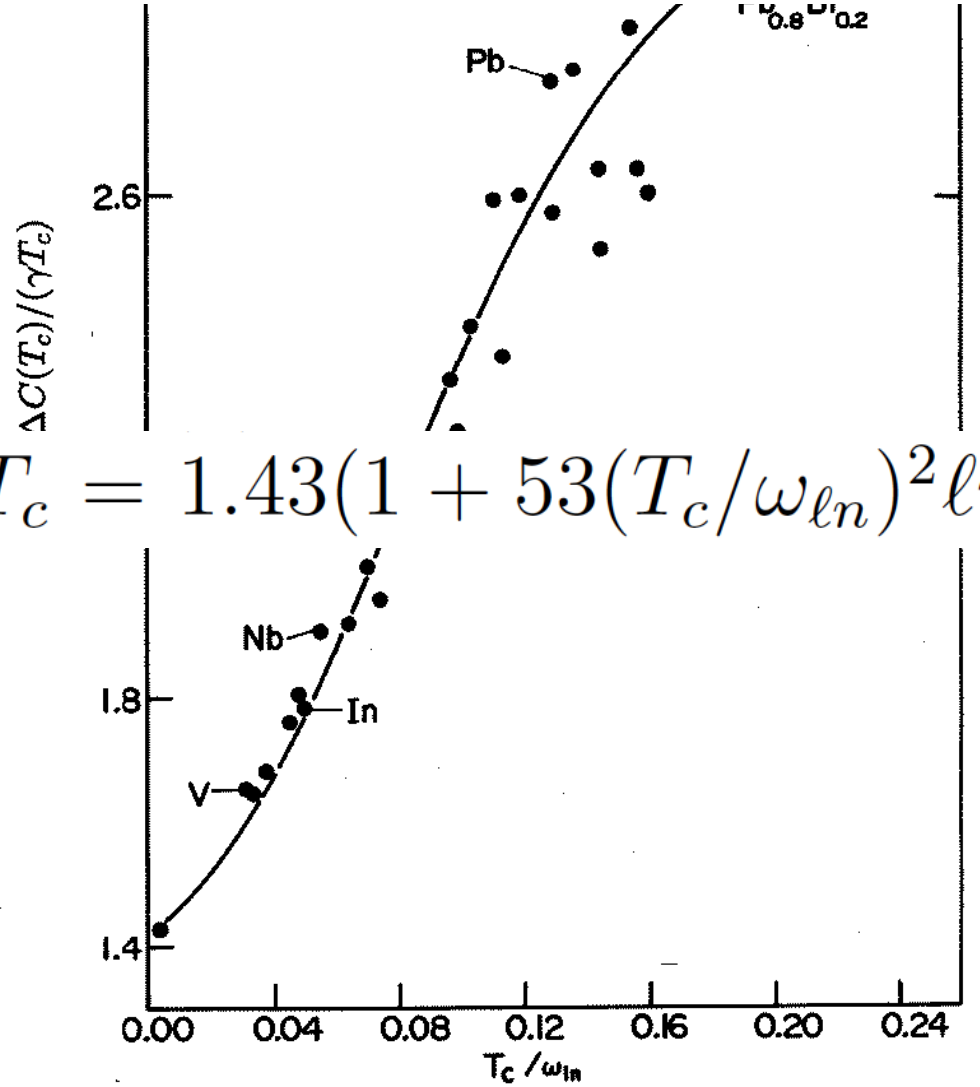

$$\Delta C(T_c)/\gamma T_c = 1.43(1 + 53(T_c/\omega_{\ell n})^2 \ell n(\omega_{\ell n}/3T_c))$$

Optical Conductivity

BCS Theory

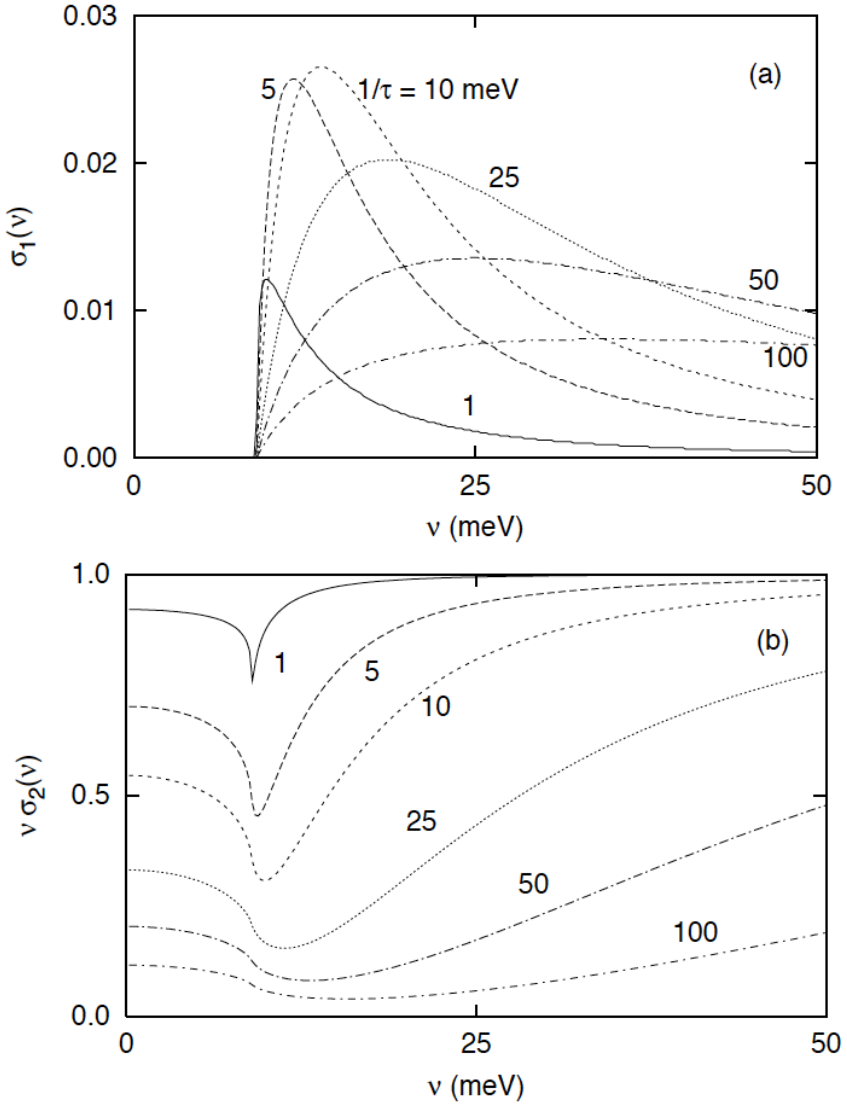

Figure 28: (a) $\sigma_1(\nu)$ vs. ν in the zero temperature BCS superconducting state for the various impurity scattering rates indicated. The absorption onset at $2\Delta(0)$ remains sharp independent of the scattering rate. A delta-function contribution (not shown) is also present at the origin. (b) Same as in (a) except for the frequency times the imaginary part of the conductivity. The optical gap is a little less evident in the dirty limit. The conductivity is given in units of $ne^2/m \equiv \omega_P^2/4\pi$). Taken from Ref. [181].

Optical Conductivity

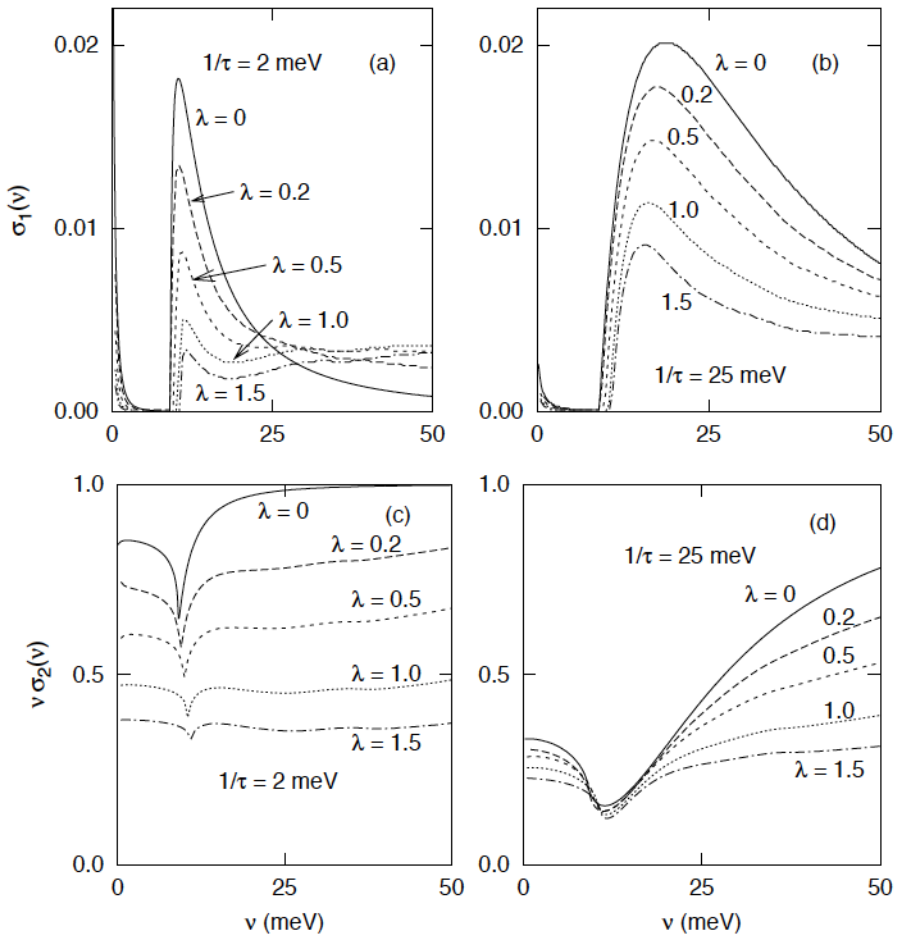

Eliashberg Theory

Figure 34: The real part (a,b) and the imaginary part (c,d) of the conductivity at essentially zero temperature ($T/T_c = 0.3$) with $1/\tau = 2$ meV (a,c) and $1/\tau = 25$ meV (b,d). In all cases we have used the BKBO spectrum scaled to give the designated value of, λ, while T_c is held fixed at 29 K by adjusting μ^*. Increased coupling strength suppresses both $\sigma_1(\nu)$ and $\nu\sigma_2(\nu)$ and broadens the minimum in the latter at 2Δ. Note that 2Δ increases slightly as the coupling strength is increased. The conductivity is given in units of $ne^2/m \equiv \omega_P^2/4\pi$).

Far-Infrared Absorption in Thin Superconducting Lead Films*

LEIGH HUNT PALMER†
Department of Physics, University of California, Berkeley, California
AND
M. TINKHAM‡

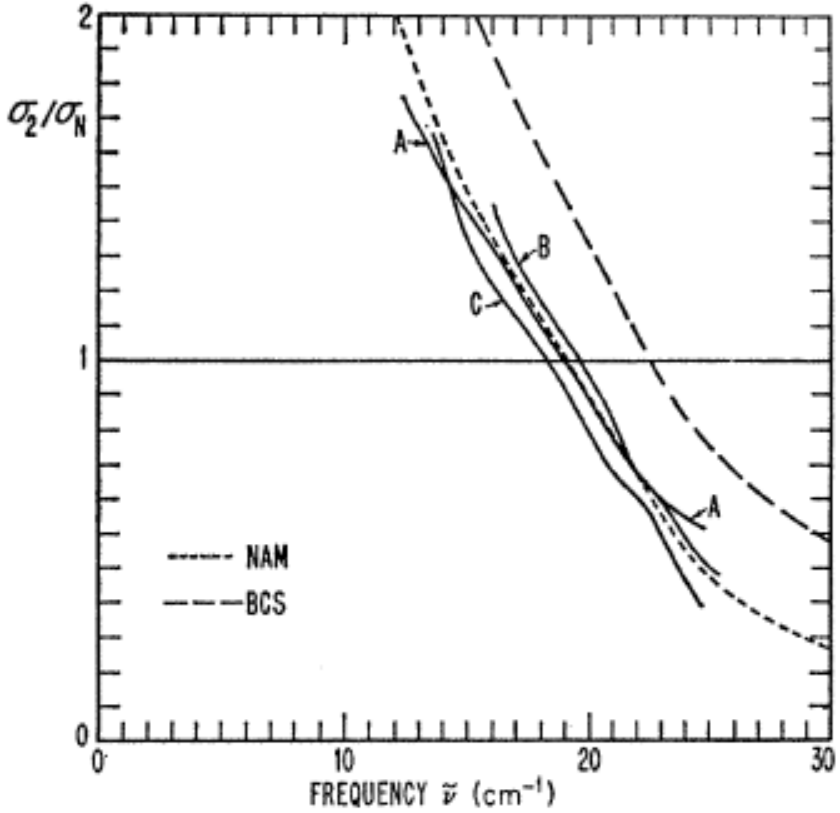

FIG. 6. Smoothed results of measurements of the imaginary part of the normalized conductivity of three lead films (A, B, and C) at 2°K. Curve labeled BCS is the weak-coupling result of Mattis and Bardeen, while that labeled Nam presents a revised version of a curve shown in Ref. 5. In both cases, the gap frequency was taken to be 22.5 cm^{-1}.

Eliashberg Theory

- Extension of BCS formalism to include dynamical electron-phonon interaction
- builds on Migdal theory in the normal state
- loosely modeled in BCS theory

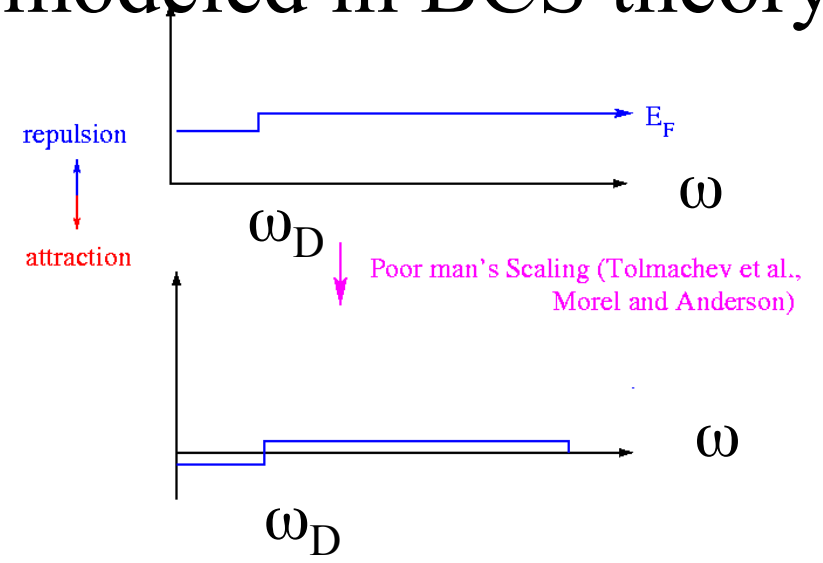

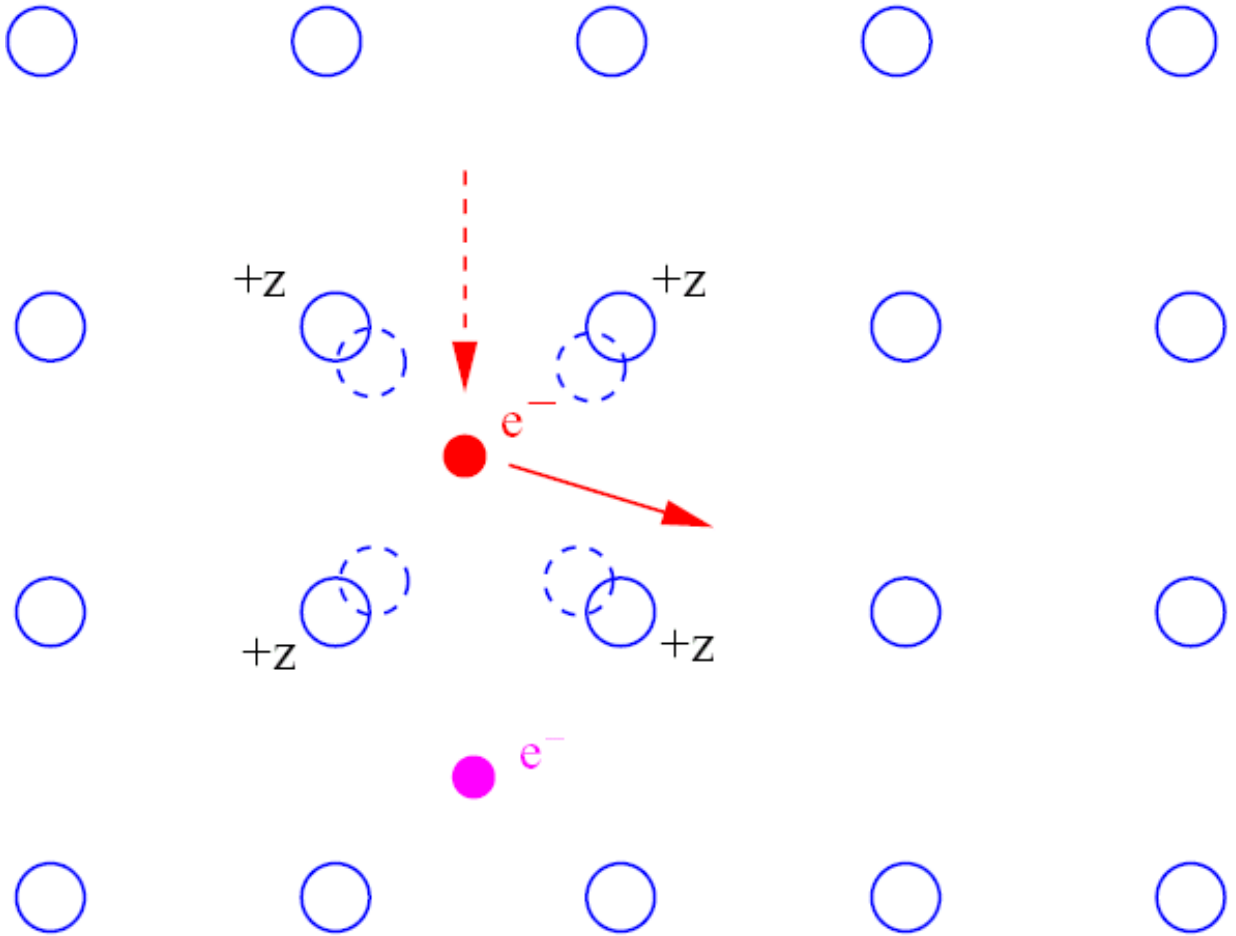

effective attraction

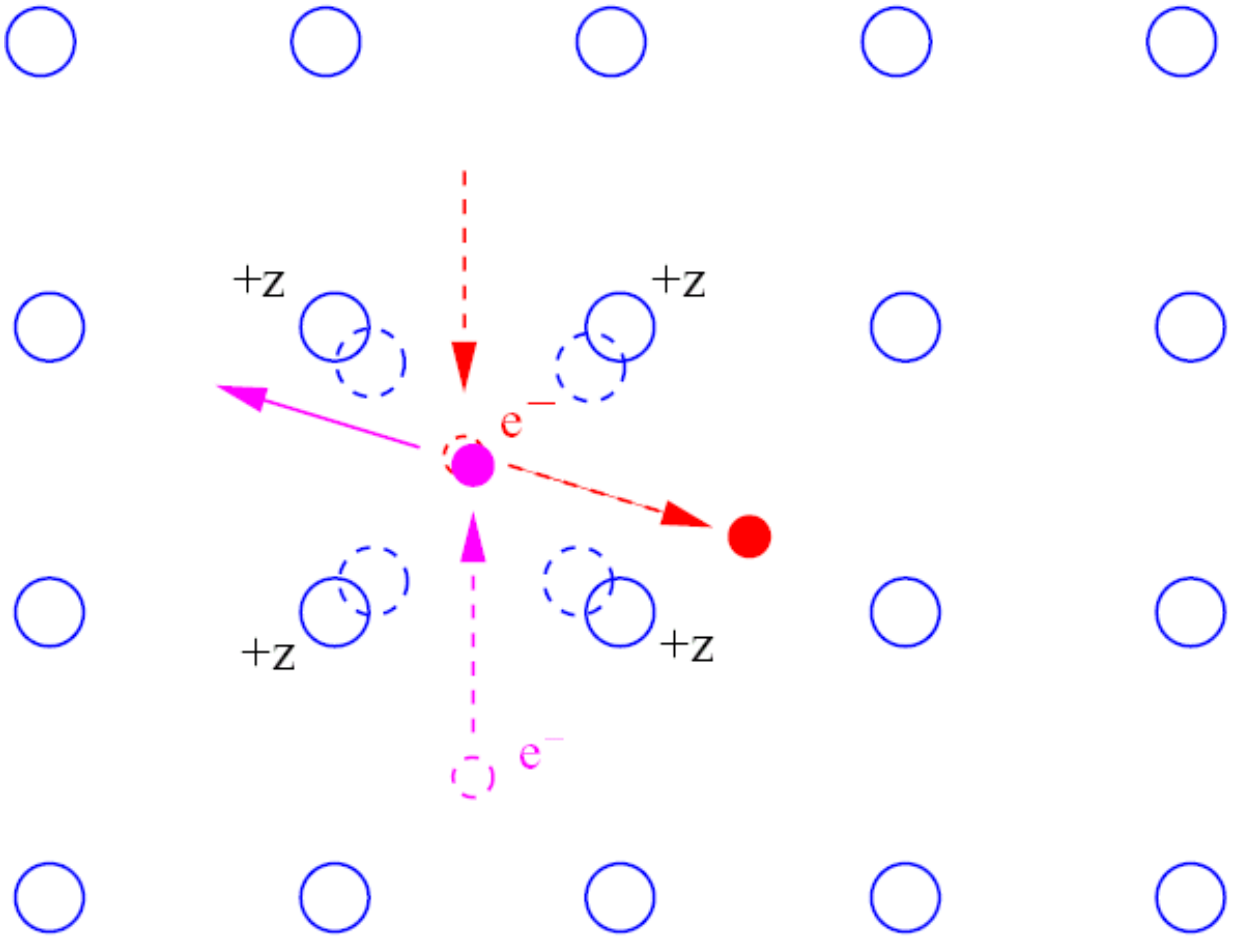

effective attraction

Measurement of $\alpha^2F(\omega)$

1) measure structure in dI/dV accurately

2) "guess" $\alpha^2F(\omega)$

3) compute, using Eliashberg theory, $\frac{dI(\omega)}{dV}$

4) correct trial $\alpha^2F(\omega)$, using functional derivatives

5) iterate until calculated dI/dV agrees with experimental one

- structure beyond phonon region
- agrees fairly well with phonon density of states
- gap ratio comes out right
- mass enhancement comes out right
- agrees with thermodynamics

BUT, complexity of Coulomb repulsion is buried in one number, μ^*